pH Reversibly Switchable Nanocapsule for Bacteria-Targeting Near-Infrared Fluorescence Imaging-Guided Precision Photodynamic Sterilization

Xu Zhao,* Kai-Chao Zhao, Li-Jian Chen, Yu-Shi Liu, Jia-Lin Liu, and Xiu-Ping Yan*

Read Online

ACCESS | Metrics & More | Article Recommendations | Supporting Information

ABSTRACT: Photodynamic sterilization is the most promising method to combat bacterial infection, especially multidrug-resistant bacterial infection. However, the absorption of conventional photosensitizers is mostly located in the UV−vis region, leading to limited penetration depth and poor therapeutic efficacy for deep-tissue bacterial infection. Besides, most of the photosensitizers are always in the activated state and lack bacteria-targeting ability, which inevitably causes severe nonspecific damage to normal tissues. Here, we show the design of a pH reversibly switchable near-infrared photosensitizer-based nanocapsule for precision bacteria-targeting fluorescence imaging-guided photodynamic sterilization. pH reversibly activatable asymmetric cyanine was synthesized as a bacteria-specific imaging unit and smart photosensitizer to realize precision imaging-guided targeting sterilization without side effects. An allicin mimic was introduced into the smart photosensitizer as the auxiliary bactericidal group to further enhance antibacterial efficiency. Meanwhile, amphipathic functionalized polyethylene glycol was employed to fabricate the nanocapsule by self-assembly to endow the charge-reversed intelligent targeting ability and prolong blood circulation. The developed switchable nanocapsule not only enables precision bacterial infection-targeted imaging without background fluorescence interference but also gives an efficient bactericidal effect with excellent specificity and negligible side effects, holding great potential for practical application.

KEYWORDS: pH reversible response, charge reversal targeting, smart nanocapsule, near-infrared fluorescence imaging, precision photodynamic sterilization
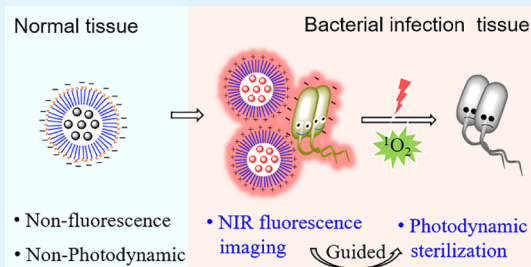
INTRODUCTION

Bacterial infection, one of the most serious threats to human health, causes a huge medical and financial burden to our society.[1,2] Antibiotics can effectively inhibit the growth of bacteria and are the most accepted treatment for bacterial infection.[3] However, the inappropriate use or even the overuse of antibiotics makes multidrug-resistant bacterial strains constantly emerge, leading to severe antibiotic resistance and high mortality.[4−7] Therefore, revolutionary antibacterial strategies with no side effects and impossibility to become drug resistance are of great necessity.

Photodynamic therapy (PDT) is expected to become a new antibacterial method because of its local and noninvasive nature, low side effects, and no drug resistance.[8−11] A photosensitizer is a key factor for PDT to produce reactive oxygen species to damage bacteria by lethal oxidative stress.[12] However, the absorption of conventional photosensitizers is mostly located in the UV−vis region, leading to limited penetration depth and poor therapeutic efficacy for deep-tissue bacterial infection.[13−16] Some efforts have been devoted to develop near-infrared (NIR) photosensitizers to overcome the abovementioned shortcoming.[17−19] However, previous NIR photosensitizers are always in the activated state and lack

bacteria-targeting ability, inevitably causing severe nonspecific damage to normal tissues. Besides, the hydrophobicity and the short cycle metabolism time of micromolecular photosensitizers often limit their therapeutic efficacy.[20−23] Hence, huge challenges remain in developing intelligent activatable NIR photosensitizers with precision bacteria-targeting and excellent antibacterial efficiency.

One of the traditional targeting strategies mainly relies on the electrostatic interaction between the cationic targeting ligands and the negatively charged surface of microbial cells.[24−26] However, positively charged nanoparticles are not good for blood circulation.[25−29] Low oxygen tension can trigger the anaerobic fermentation in certain bacteria to produce organic acids and make the infected site acidic (ca. pH 5.5).[30] This feature enables the development of the charge-
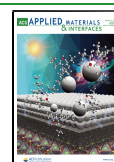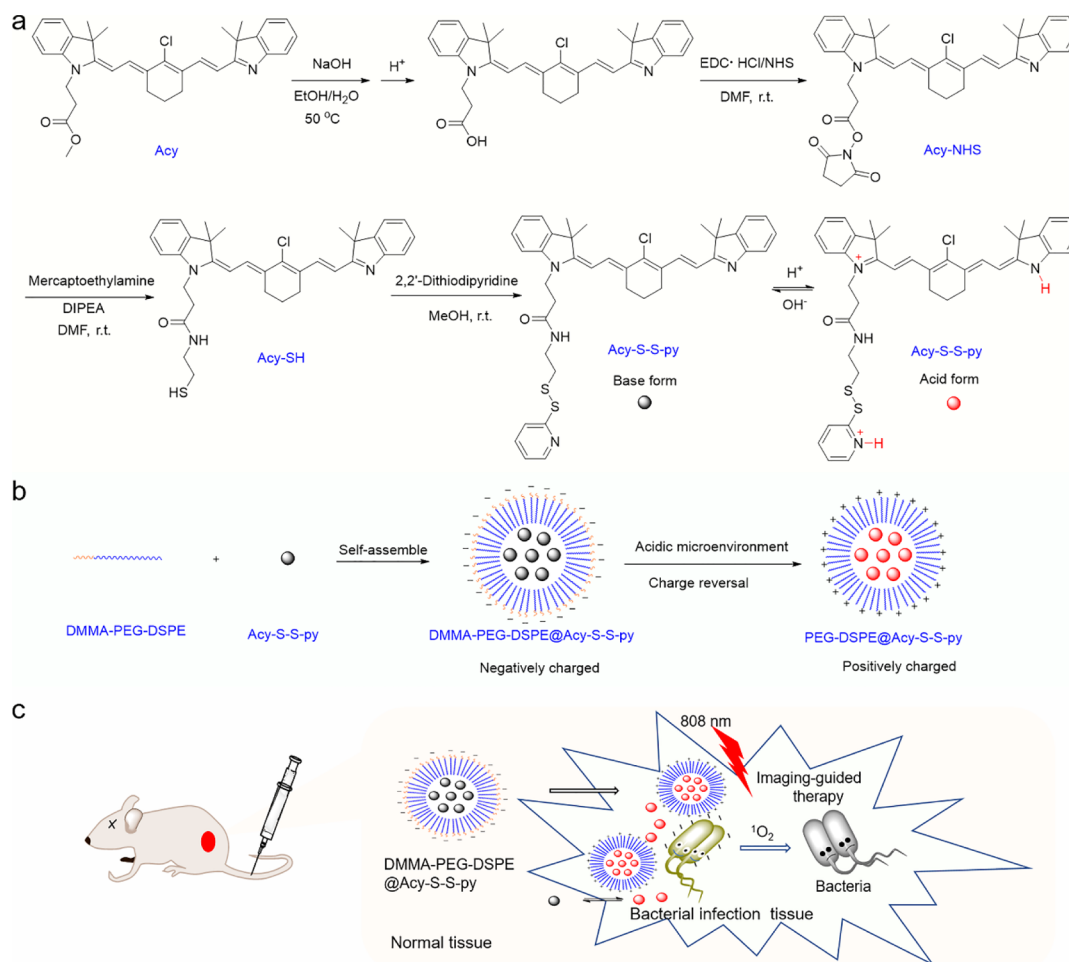
Figure 1. (a) Schematic for the design and synthesis of the Acy-S-S-Py photosensitizer. (b) Schematic for the design and preparation of the DSPE-PEG-DMMA@Acy-S-S-Py nanocapsule. (c) Illustration of DSPE-PEG-DMMA@Acy-S-S-Py as a pH reversibly switchable theranostic platform for precision bacteria-targeting NIR fluorescence imaging-guided smart photodynamic sterilization.

conversion "smart" targeting strategy to simultaneously meet the requirements of both blood circulation and bacteria-targeting ability.[30−32]

Herein, we report a rational design of the pH reversibly switchable nanocapsule for smart bacteria-targeting NIR fluorescence imaging-guided precision photodynamic sterilization. pH reversibly activated asymmetric cyanine (Acy) is synthesized as both the activatable fluorescence imaging unit and photosensitizer for precision bacteria-targeting fluorescence imaging-guided photodynamic sterilization. The pyridinyldithio group (-S-S-Py), the mimic of allicin,[33] is introduced as an auxiliary bactericidal group to further enhance the antibacterial effect (Acy-S-S-Py). Meanwhile, distearyl phosphatidyl ethanolamine (DSPE)- and 2,3-dimethylmaleic anhydride (DMMA)-functionalized polyethylene glycol (PEG) (DSPE-PEG-DMMA) is designed to fabricate the DSPE-PEG-DMMA@Acy-S-S-Py nanocapsule via self-assembly, endowing charge-reversed smart targeting ability and long blood circulation. The as-prepared DSPE-PEG-DMMA@Acy-S-S-Py nanocapsule not only enables precision bacterial infection-targeted imaging with a high signal-to-background ratio (S/B) but also gives rapid and strong bactericidal effects with super specificity and negligible side effects, holding great potential for practical application.

RESULTS AND DISCUSSION

Design, Synthesis, and Characterization of DSPE-PEG-DMMA@Acy-S-S-Py. The design and synthesis of the DSPE-PEG-DMMA@Acy-S-S-Py nanocapsule for precision bacteria-targeting fluorescence imaging-guided smart photodynamic sterilization are illustrated in Figure 1. The synthesis of the DSPE-PEG-DMMA@Acy-S-S-Py nanocapsule started from Acy. Here, Acy, a non-N-alkylated asymmetric cyanine molecule, was explored as the mother molecule owing to its unique property of pH-reversible absorption and fluorescence emission.[34] Density functional theory (DFT) calculation shows that Acy also has great potential to produce singlet oxygen ($^1O_2$) under an acidic microenvironment (Figure 2a,b). Thus, Acy was designed as both the pH-reversibly activatable imaging unit and smart photosensitizer to realize precision bacteria-targeting imaging and imaging guided smart photodynamic sterilization. The -S-S-Py group was then introduced into Acy as the auxiliary bactericidal group to inhibit the activity of thiol protease for further enhancement of the antibacterial effect.[33] For this purpose, Acy was hydrolyzed and became active succinimide ester of Acy (Acy-NHS) via amide condensation with 1-ethyl-3-(3-dimethylaminopropyl)carbodiimide hydrochloride (EDC·HCl) and N-hydroxysuccinimide (NHS) as the condensation reagent. Acy-NHS was then reacted with mercaptoethylamine to form -SH-functionalized Acy (Acy-
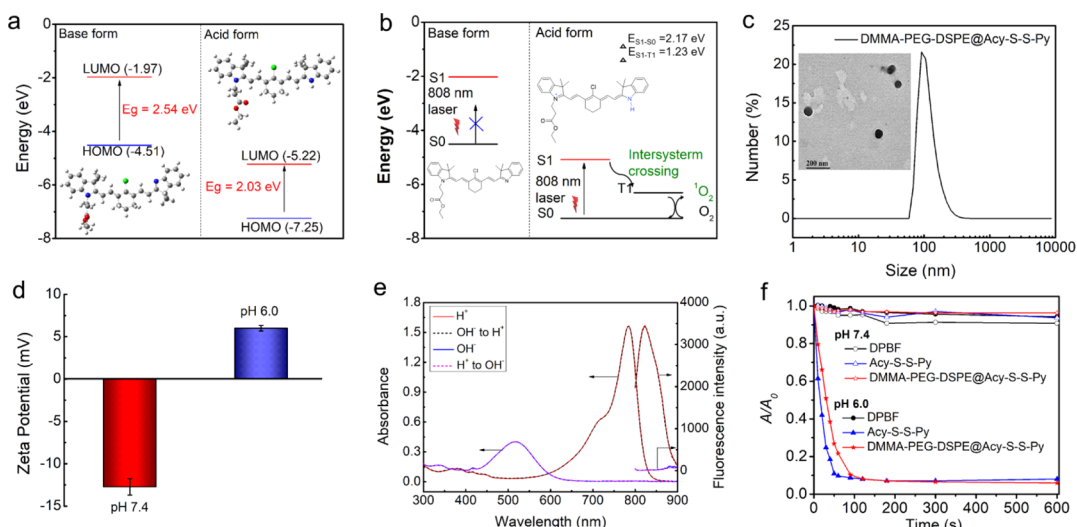
Figure 2. Characterization of the prepared DSPE-PEG-DMMA@Acy-S-S-Py nanocapsule: (a) optimized structures and frontier molecular orbital (HOMO and LUMO) energies based on DFT calculations (Gaussian 09/6-31G(d)) of Acy in its ground state (S0). (b) Schematic for $^1O_2$ generation with Acy (S1: lowest excited singlet state and T1: lowest excited triplet state.). (c) Hydrodynamic diameter distribution of the DSPE-PEG-DMMA@Acy-S-S-Py nanocapsule. The inset shows the transmission electron microscopy images of the DSPE-PEG-DMMA@Acy-S-S-Py nanocapsule. (d) Zeta potentials of the DSPE-PEG-DMMA@Acy-S-S-Py nanocapsule at pH 6.0 and 7.4. (e) pH-reversible UV−vis−NIR absorption and fluorescence spectra of Acy-S-S-Py (1×10^{-5} M) at pH 7.4 and 6.0. (f) Time-dependent absorbance of DPBF (A/A_0) at 410 nm with and without Acy-S-S-Py or DSPE-PEG-DMMA@Acy-S-S-Py (5×10^{-6} M as Acy-S-S-Py) at pH 6.0 and 7.4 under continuous 808 nm laser irradiation. A and A_0 are the absorbance of DPBF at a certain irradiation time and before irradiation, respectively.
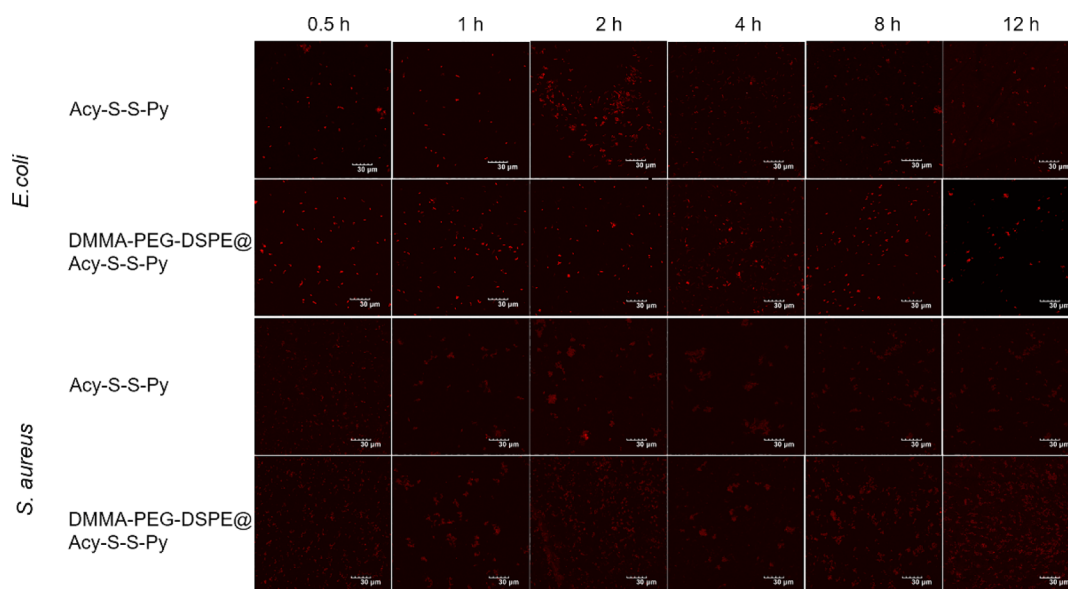
Figure 3. CLSM images of *E. coli* and *S. aureus* incubated with DSPE-PEG-DMMA@Acy-S-S-Py or Acy-S-S-Py (5×10^{-6} M as Acy-S-S-Py). The scale bar is 30 μm.

SH). Acy-SH provided -SH terminal to further react with 2,2′-dithiodipyridine via a nucleophilic substitution to offer -S-S-Py-modified Acy (Acy-S-S-Py) (Figures S1−S6). Finally, amphiphilic polymer DSPE-PEG-DMMA was employed as the smart targeting group and self-assemble unit to further form the pH-switchable nanocapsule (DSPE-PEG-DMMA@Acy-S-S-Py) to realize charge-conversion smart targeting capability and prolong blood circulation.

The as-prepared DSPE-PEG-DMMA@Acy-S-S-Py nanocapsule is presented as a well-dispersed and homogenous sphere with a particle size of 40.0 ± 3.2 nm and an average hydrate diameter of 110.3 ± 3.1 nm (Figure 2c). Change in pH from 7.4 to 6.0 did not influence the morphological and hydrate diameter of DSPE-PEG-DMMA@Acy-S-S-Py but made the zeta potential change from negative (−12.7 ± 1.0 mV) into positive (6.0 ± 0.3 mV) (Figure 2d) because of the detachment of DMMA from DSPE−PEG−MMMA and protonation of exposed DSPE-PEG-NH$_2$ residue. The results indicate that the as-synthesized DSPE-PEG-DMMA@Acy-S-S-Py has pH-mediated charge-conversion feature, laying a solid foundation for smart bacteria-targeting ability and long blood circulation. Besides, the prepared DSPE-PEG-DMMA@Acy-S-S-Py offered excellent colloidal stability in a simulated complex physiological medium (Figure S7), which is beneficial for practical application.
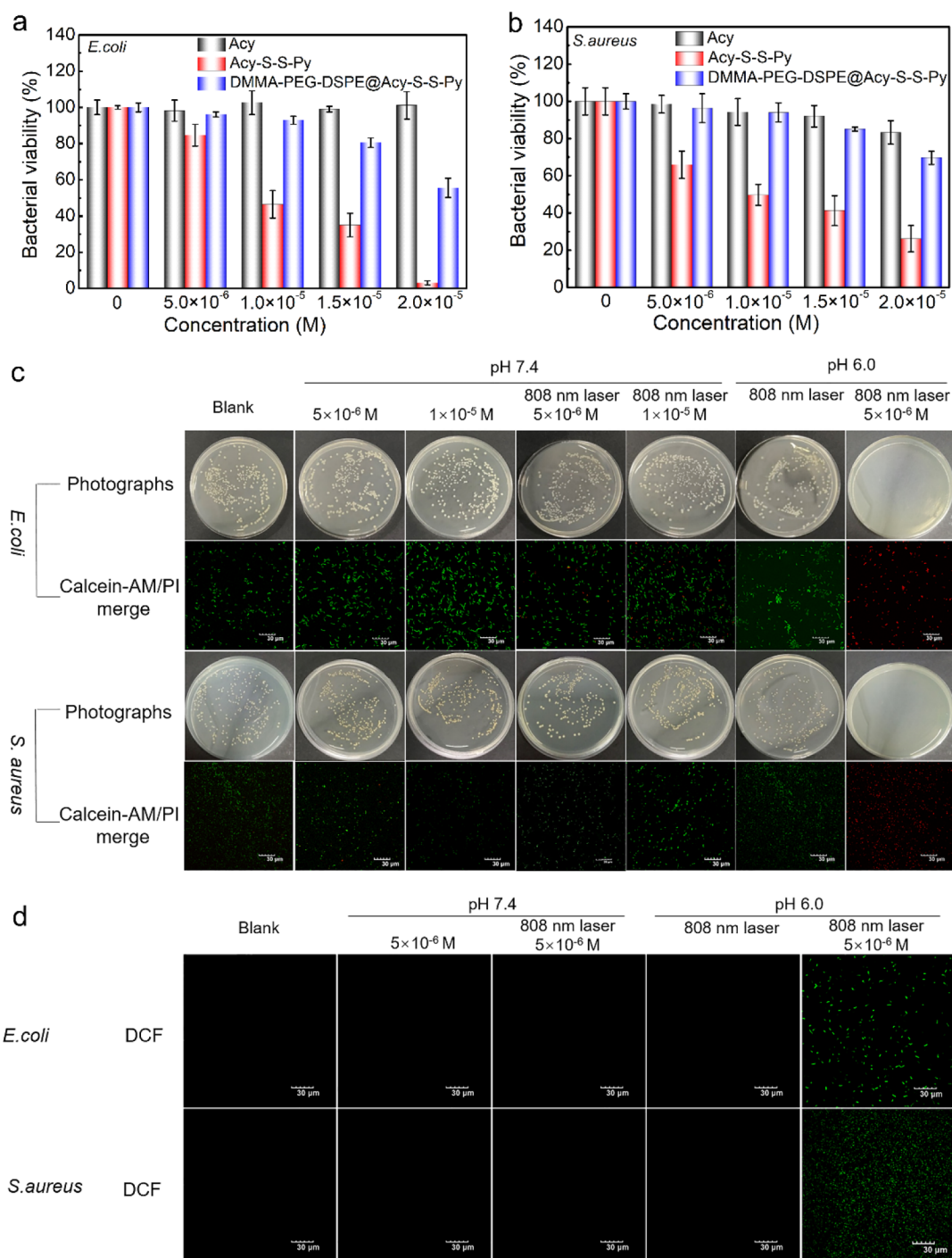
Figure 4. Dark toxicity and photodynamic sterilization effect: (a) dark toxicity of Acy, Acy-S-S-Py, and DSPE-PEG-DMMA@Acy-S-S-Py to *E. coli*. (b) Dark toxicity of Acy, Acy-S-S-Py, and DSPE-PEG-DMMA@Acy-S-S-Py to *S. aureus*. (c) Representative flat colony photographs and CLSM images (Calcein-AM/PI live-dead bacterial staining) of bacterial colonies treated in different ways (Calcein-AM: green fluorescence, live bacteria and PI: red fluorescence, dead bacteria). (d) CLSM images of bacterial colonies treated in different ways for the detection of cytosolic $^1O_2$ (λex = 488 nm, λem = 500−600 nm, blue fluorescence of DCF represents $^1O_2$ production).

Acy-S-S-Py gave a characteristic absorption peak at *ca.* 515 nm at simulated normal physiological pH (pH 7.4) but showed a new characteristic peak at *ca.* 785 nm in conjunction with an obvious decreased original peak at 515 nm in simulated bacterial acidic microenvironment (pH 6.0) and vice versa (Figure 2e). Besides, simulated bacterial acidic microenvironment also enabled the NIR fluorescence of Acy-S-S-Py with a characteristic emission peak at 820 nm to be activated (Figure 2e) because of the intramolecular charge transfer process

originating from the protonation of the indole ring *N* atoms. The pk_a and the pH sensitive range of Acy-S-S-Py were determined to be 5.8 and 4.5−7.5, respectively, by fluorescence titration (Figure S8), matching well with the bacterial acidic microenvironment. Self-assembly of DSPE-PEG-DMMA and Acy-S-S-Py did not affect the intrinsic pH reversibly activated absorption and fluorescence features of Acy-S-S-Py (Figure S9) but enhanced the photostability of Acy-S-S-Py, especially under an acidic microenvironment (Figure S10). The content
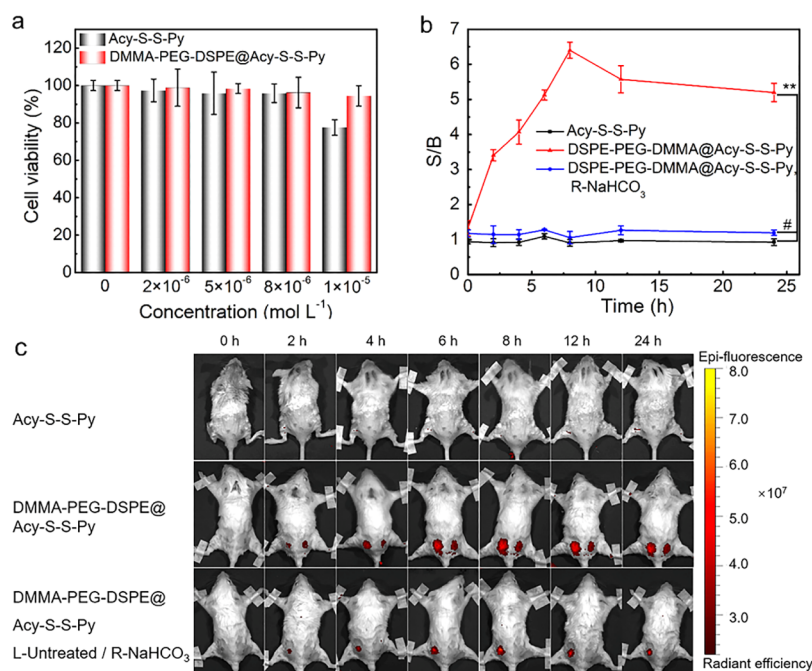
Figure 5. Cell cytotoxicity and *in vivo* imaging performance of DSPE-PEG-DMMA@Acy-S-S-Py: (a) viability of NIH-3T3 cells incubated with DSPE-PEG-DMMA@Acy-S-S-Py. (b) Signal-to-background ratio (S/B) of infected site of *S. aureus*-infected mice after intravenous injection of DSPE-PEG-DMMA@Acy-S-S-Py or Acy-S-S-Py ($n = 3$) as a function of time (statistical significance: **, $P < 0.001$; #, not significant). (C) NIR fluorescence imaging of *S. aureus*-infected mice intravenously injected with DSPE-PEG-DMMA@Acy-S-S-Py or Acy-S-S-Py at different time points post injection.

of Acy-S-S-Py loaded into the DSPE-PEG-DMMA@Acy-S-S-Py nanocapsule was measured to be 2.93×10^{-4} mol g^{-1} by UV−vis−NIR absorption spectrometry. The pH reversible response feature and good photostability of the as-prepared DSPE-PEG-DMMA@Acy-S-S-Py nanocapsule provide the possibility for bacterial acidic microenvironment-specific activated imaging and photodynamic sterilization.

Acid-Activated Photodynamic Performance of DSPE-PEG-DMMA@Acy-S-S-Py. We then evaluated the acid-activated photodynamic performance of DSPE-PEG-DMMA@Acy-S-S-Py by evaluating its capability for $^1O_2$ generation. 1,4-Diphenyl-2,3-benzofuran (DPBF) was chosen to probe $^1O_2$ because $^1O_2$ oxidation leads to the decrease in the absorbance of DPBF.[35] DSPE-PEG-DMMA@Acy-S-S-Py (pH 6.0) under 808 nm laser irradiation (0.6 W cm^{-2}) generated obvious $^1O_2$ as confirmed by the significant decrease in the absorbance of DPBF (Figures 2f and S11e). The generation efficiency of DSPE-PEG-DMMA@Acy-S-S-Py was similar to that of Acy-S-S-Py with the same concentration (as Acy-S-S-Py) at pH 6.0 (Figures 2f and S11e cf. Figure S11c). In contrast, neither DSPE-PEG-DMMA@Acy-S-S-Py or Acy-S-S-Py (pH 7.4) nor DBPF alone (pH 7.4 and 6.0) produced any $^1O_2$ as confirmed by the constant absorbance of DPBF during 10 min 808 nm laser irradiation with the same power density (Figures 2f and S11a,b,d,f). The abovementioned results show that DSPE-PEG-DMMA@Acy-S-S-Py enables efficient generation of $^1O_2$ only in the acidic environment. The distinct pH reversible response and weak acidity specifically activated PDT effect make DSPE-PEG-DMMA@Acy-S-S-Py have great potential for precision photodynamic sterilization with excellent bacterial specificity.

In Vitro Imaging and Antimicrobial Performance of DSPE-PEG-DMMA@Acy-S-S-Py. The abovementioned results encouraged us to explore DSPE-PEG-DMMA@Acy-S-S-

Py as a photodynamic antibacterial agent against *Escherichia coli* (*E. coli*, representatives of Gram-negative) and *Staphylococcus aureus* (*S. aureus*, representatives of Gram-positive bacteria). The optimal incubation time was investigated using confocal laser scanning microscopy (CLSM) (Figure 3). CLSM imaging results show that DSPE-PEG-DMMA@Acy-S-S-Py rapidly aggregated on the *E. coli*, and the fluorescence signal was lightened up with the maximum at *ca.* 1−2 h and kept constant up to at least 12 h. However, the fluorescence signal of *E. coli* in the Acy-S-S-Py group reached the maximum at *ca.* 2 h and then rapidly decreased with metabolism. Similar phenomena were also found for *S. aureus*. These results indicate that the bacteria-targeting ability and the metabolic rate were significantly improved by DSPE-PEG-DMMA, and 2 h is the most appropriate incubation time for the follow-up photodynamic sterilization.

Dark toxicity and photodynamic sterilization effect of DSPE-PEG-DMMA@Acy-S-S-Py was evaluated using the flat colony counting method and calcein acetoxymethyl ester (Calcein-AM)/propidium iodide (PI) live-dead bacterial staining method. DSPE-PEG-DMMA@Acy-S-S-Py had good bacterial compatibility against *E. coli* and *S. aureus* because more than 80% of *E. coli* and *S. aureus* still survived even in the presence of DSPE-PEG-DMMA@Acy-S-S-Py with 1×10^{-5} M (as Acy-S-S-Py), obviously superior to Acy-S-S-Py at the same concentration. Besides, compared with Acy, Acy-S-S-Py showed certain bactericidal activity on both *E. coli* and *S. aureus* in a dose-dependent manner (Figure 4a,b). These results confirm that the introduction of DSPE-PEG-DMMA enhanced the biocompatibility of Acy-S-S-Py, and the S-S-Py group did have auxiliary antibacterial activity.

An extremely low bacterial viability (*ca.* 0%) was observed for both *E. coli* and *S. aureus* treated with lower concentration of DSPE-PEG-DMMA@Acy-S-S-Py (5×10^{-6} M as Acy-S-S-
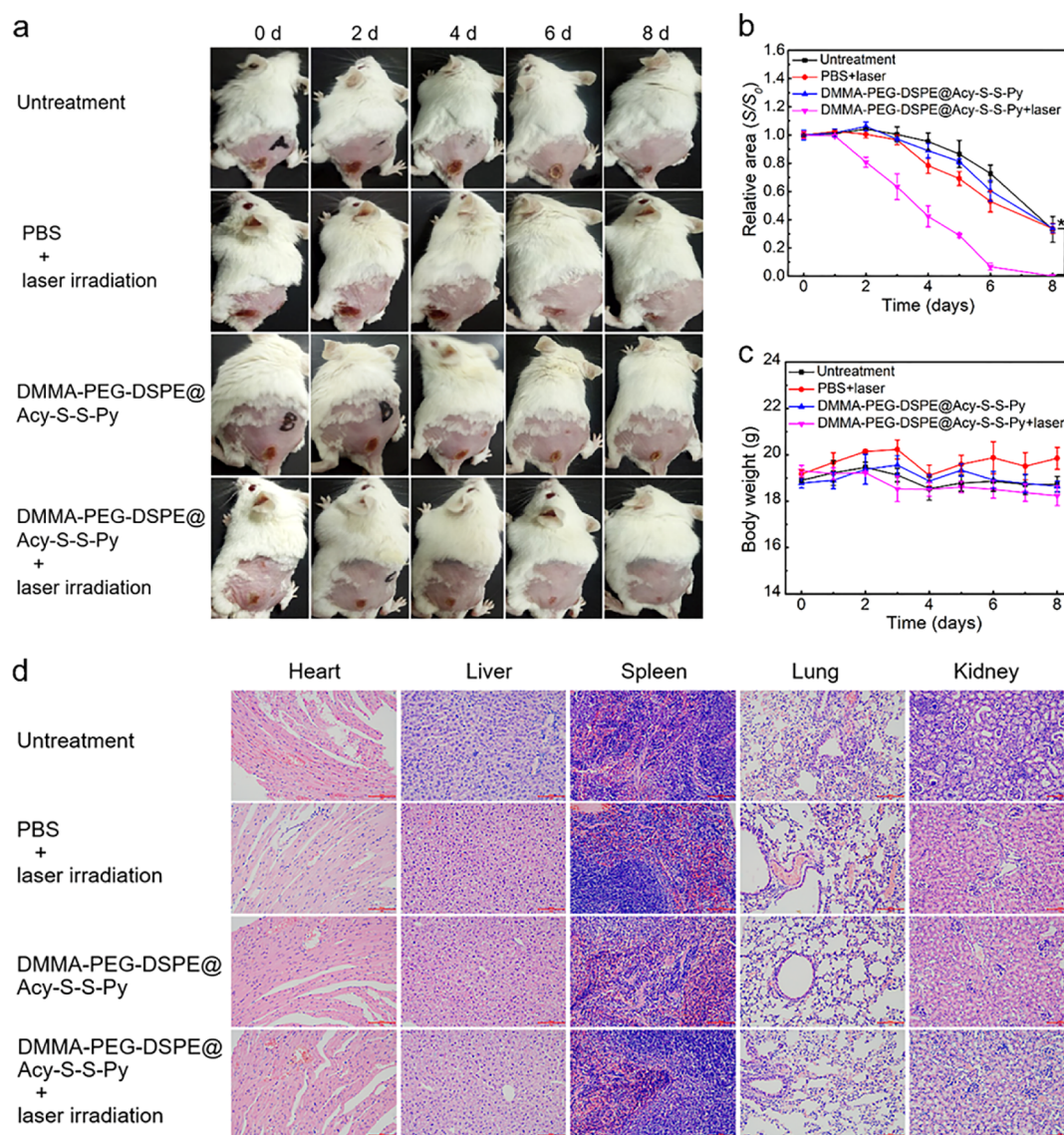
Figure 6. DSPE-PEG-DMMA@Acy-S-S-Py-mediated *in vivo* photodynamic sterilization in *S. aureus* infection-bearing mice models: (a) representative photographs for different groups of mice. (b) Time-dependent relative area of infected wound for different groups of mice. S_0 is the initial area of infected wound, while S is the area of infected wound at a certain therapy point (statistical significance: *, $P < 0.01$). (c) Body weight change of different groups of mice with time. (d) H&E staining of main organs of control and treatment groups of mice after treatment. The scale bar is 50 μm.

Py) at pH 6.0 under 808 nm laser irradiation (0.6 W cm^{-2}) for 10 min (Figure 4c). In contrast, higher concentration of DSPE-PEG-DMMA@Acy-S-S-Py (1×10^{-5} M) at pH 7.4 did not induce discernible influence on both *E. coli* and *S. aureus*, whether with 808 nm laser irradiation or not. Besides, only 808 nm laser irradiation at pH 6.0 exhibited a negligible antibacterial effect. These results clearly show that the photodynamic sterilization effect of DSPE-PEG-DMMA@Acy-S-S-Py could merely be activated at the acidic microenvironment, ensuring specific and efficient antibacterial effects with no side effect to adjacent normal tissues.

To further confirm the photodynamic sterilization effect of DSPE-PEG-DMMA@Acy-S-S-Py, 2′,7′-dichlorodihydrofluorescein diacetate (DCFH-DA) was employed as the cytosolic $^1O_2$ probe in bacterial imaging as it can be oxidized by cytosolic $^1O_2$ to 2′,7′-dichlorofluorescein (DCF) with strong green fluorescence.[36] No fluorescent signal was observed in the bacteria of control groups (without any treatments, treated with DSPE-PEG-DMMA@Acy-S-S-Py whether 808 nm laser irradiation or not at pH 7.4 and 808 nm laser irradiation at pH 6.0). However, obvious green fluorescence was lightened up in the bacteria treated with DSPE-PEG-DMMA@Acy-S-S-Py upon 808 nm laser irradiation at pH 6.0 (Figure 4d), indicating that antibacterial activity of DSPE-PEG-DMMA@Acy-S-S-Py was related to the formation of $^1O_2$ and exhibited a pH-dependent manner.

***In Vivo* Bacterial Infection-Targeting NIR Imaging and Precision Photodynamic Sterilization.** We then explore the potential of DSPE-PEG-DMMA@Acy-S-S-Py for *in vivo* precision imaging and imaging-guided smart photodynamic sterilization. To this end, the biocompatibility of DSPE-PEG-DMMA@Acy-S-S-Py was first evaluated using mouse embryonic fibroblast (NIH-3T3) cells as model cells. The cell viability of NIH-3T3 remained over 92% even in the presence of DSPE-PEG-DMMA@Acy-S-S-Py up to 1×10^{-5} M, significantly higher than that (*ca.* 79%) in the presence of

Acy-S-S-Py at the same concentration (Figure 5a), demonstrating that the as-prepared DSPE-PEG-DMMA@Acy-S-S-Py has good biocompatibility and the self-assembly strategy is helpful to improve biocompatibility.

In vivo precision bacterial infection-targeting imaging performance of DSPE-PEG-DMMA@Acy-S-S-Py was subsequently investigated through intravenously injecting DSPE-PEG-DMMA@Acy-S-S-Py (experiment group) or Acy-S-S-Py (control group) into the *S. aureus* infection-bearing mice (Figure 5b,c). The NIR fluorescence signal appeared only in the infected sites of the experimental group at *ca.* 2 h after injection and gradually increased to the maximum at *ca.* 8 h and then almost kept constant up to at least 24 h, indicating that DSPE-PEG-DMMA@Acy-S-S-Py has precision bacterial infection targetability and the maximum accumulation in the infected sites at 8 h post-injection. Therefore, 8 h was taken as the most appropriate time for the follow-up therapy. In contrast, no fluorescence signal was observed in the control group and other sites except for infected sites of the experimental group during the whole process. For comparison, another experiment group was in situ-injected $NaHCO_3$ into the right infection site 30 min before the intravenous injection of DSPE-PEG-DMMA@Acy-S-S-Py to break the acidic microenvironment. The fluorescence signal in left infection was lightened up as usual and still kept clear up to at least 24 h, while no fluorescence signal appeared in the $NaHCO_3$-treated right infection and other normal tissues. These results clearly show that the fluorescence activation of DSPE-PEG-DMMA@Acy-S-S-Py was specifically governed by the bacterial infection acidic microenvironment and the bacteria-targeting ability was significantly improved by DSPE-PEG-DMMA and the self-assembly strategy. The abovementioned results also indicate that DSPE-PEG-DMMA@Acy-S-S-Py is competent for precision bacterial infection-targeting imaging without background interference.

To evaluate *in vivo* photodynamic sterilization effect of DSPE-PEG-DMMA@Acy-S-S-Py, we established a subcutaneous infection model in mice by injecting *S. aureus*. The *S. aureus*-infected mice were randomly divided into four groups (three mice/group). The infected mice which were intravenously injected with DSPE-PEG-DMMA@Acy-S-S-Py (100 μL, 2.5×10^{-5} mol L^{-1} as Acy-S-S-Py) and subjected to 10 min 808 nm laser irradiation (0.6 W cm^{-2}) at 8 h postinjection were assigned as the treatment group, while the other infected mice treated with PBS with 808 nm laser exposure and injected with DSPE-PEG-DMMA@Acy-S-S-Py without laser irradiation and without any treatment acted as three control groups. The treatment group showed alleviated infection and faster healing compared to the control groups, and the infected wounds were completely re-epithelialized at *ca.* 8 d (Figure 6a,b). No significant difference was observed in the infection healing rate among the control groups. Neither significant body weight change nor behavior disorder was observed in all experimental mice during the whole observation process (Figure 6c). Besides, no noticeable organ necrosis or inflammation was observed in both treatment and control groups (Figure 6d). These results reveal that the developed DSPE-PEG-DMMA@Acy-S-S-Py nanocapsule is competent for precision photodynamic sterilization with an excellent therapeutic effect and negligible side effect merely by a single intravenous injection and one-time laser irradiation.

CONCLUSIONS

In conclusion, we have reported the pH reversibly switchable DSPE-PEG-DMMA@Acy-S-S-Py nanocapsule for precision bacteria-targeting NIR fluorescence imaging-guided photodynamic sterilization. The developed nanocapsule integrated the merits of the pH reversibly activatable NIR fluorescence imaging and photodynamic sterilization of Acy, the auxiliary enhanced sterilization of -S-S-Py, and the charge reversal targeting capability and enhanced blood circulation from DSPE-PEG-DMMA. These integrated merits make DSPE-PEG-DMMA@Acy-S-S-Py overcome the shortcomings of the limited therapeutic efficiency in deep tissue infection and nonspecific damage in the previous "always on" PDT sterilization platforms. We believe that the integration of the reversibly activated imaging and photodynamic sterilization with the charge reversal targeting strategy furnishes a prospective strategy to design smart sterilization nanoplatforms for skin infection and deep tissue inflammation.

ASSOCIATED CONTENT

Ⓢ Supporting Information

The Supporting Information is available free of charge at https://pubs.acs.org/doi/10.1021/acsami.0c14063.

> Additional data including chemicals and materials, instrumentation, experimental details, characterization of Acy-S-S-Py and the intermediates, time- and solution-dependent hydrodynamic diameter of DSPE-PEG-DMMA@Acy-S-S-Py, and photostability of DSPE-PEG-DMMA@Acy-S-S-Py (PDF)

AUTHOR INFORMATION

Corresponding Authors

Xu Zhao − *State Key Laboratory of Food Science and Technology, International Joint Laboratory on Food Safety, and Institute of Analytical Food Safety, School of Food Science and Technology, Jiangnan University, Wuxi 214122, China;* ⓞ orcid.org/0000-0001-8000-9045; Email: zhaoxu2017@jiangnan.edu.cn

Xiu-Ping Yan − *State Key Laboratory of Food Science and Technology, International Joint Laboratory on Food Safety, Institute of Analytical Food Safety, School of Food Science and Technology, and Key Laboratory of Synthetic and Biological Colloids, Ministry of Education, School of Chemical and Material Engineering, Jiangnan University, Wuxi 214122, China;* ⓞ orcid.org/0000-0001-9953-7681; Email: xpyan@jiangnan.edu.cn

Authors

Kai-Chao Zhao − *Institute of Analytical Food Safety, School of Food Science and Technology and Key Laboratory of Synthetic and Biological Colloids, Ministry of Education, School of Chemical and Material Engineering, Jiangnan University, Wuxi 214122, China*

Li-Jian Chen − *State Key Laboratory of Food Science and Technology, International Joint Laboratory on Food Safety, and Institute of Analytical Food Safety, School of Food Science and Technology, Jiangnan University, Wuxi 214122, China;* ⓞ orcid.org/0000-0001-8671-8766

Yu-Shi Liu − *Institute of Analytical Food Safety, School of Food Science and Technology, Jiangnan University, Wuxi 214122, China*

Jia-Lin Liu − *Institute of Analytical Food Safety, School of Food Science and Technology and Key Laboratory of Synthetic and Biological Colloids, Ministry of Education, School of Chemical and Material Engineering, Jiangnan University, Wuxi 214122, China*

■ REFERENCES

(1) Zhao, Z.; Yan, R.; Yi, X.; Li, J.; Rao, J.; Guo, Z.; Yang, Y.; Li, W.; Li, Y.-Q.; Chen, C. Bacteria-Activated Theranostic Nanoprobes Against Methicillin-Resistant Staphylococcus Aureus Infection. *ACS Nano* **2017**, *11*, 4428−4438.

(2) Huang, J.; Zhou, J.; Zhuang, J.; Gao, H.; Huang, D.; Wang, L.; Wu, W.; Li, Q.; Yang, D.-P.; Han, M.-Y. Strong Near-Infrared Absorbing and Biocompatible CuS Nanoparticles for Rapid and Efficient Photothermal Ablation of Gram-Positive and -Negative Bacteria. *ACS Appl. Mater. Interfaces* **2017**, *9*, 36606−36614.

(3) Yang, F.; Feng, Y.; Fan, X.; Zhang, M.; Wang, C.; Zhao, W.; Zhao, C. Biocompatible Graphene-Based Nanoagent with NIR and Magnetism Dual-Responses for Effective Bacterial Killing and Removal. *Colloids Surf., B* **2019**, *173*, 266−275.

(4) Vasilev, K.; Sah, V.; Anselme, K.; Ndi, C.; Mateescu, M.; Dollmann, B.; Martinek, P.; Ys, H.; Ploux, L.; Griesser, H. J. Tunable Antibacterial Coatings That Support Mammalian Cell Growth. *Nano Lett.* **2010**, *10*, 202−207.

(5) Li, L.-L.; Xu, J.-H.; Qi, G.-B.; Zhao, X.; Yu, F.; Wang, H. Core-Shell Supramolecular Gelatin Nanoparticles for Adaptive and "On-Demand" Antibiotic Delivery. *ACS Nano* **2014**, *8*, 4975−4983.

(6) Yan, L. X.; Chen, L. J.; Zhao, X.; Yan, X. P. pH Switchable Nanoplatform for In Vivo Persistent Luminescence Imaging and Precise Photothermal Therapy of Bacterial Infection. *Adv. Funct. Mater.* **2020**, *30*, 1909042.

(7) Jiang, L.; Gan, C. R. R.; Gao, J.; Loh, X. J. A Perspective on the Trends and Challenges Facing Porphyrin-Based Anti-Microbial Materials. *Small* **2016**, *12*, 3609−3644.

(8) Kashef, N.; Huang, Y.-Y.; Hamblin, M. R. Advances in Antimicrobial Photodynamic Inactivation at the Nanoscale. *Nanophotonics* **2017**, *6*, 853−879.

(9) Shi, X.; Zhang, C. Y.; Gao, J.; Wang, Z. Recent advances in Photodynamic Therapy for Cancer and Infectious Diseases. *WIREs Nanomed. Nanobiotechnol.* **2019**, *11*, No. e1560.

(10) Hamblin, M. R.; Hasan, T. Photodynamic Therapy: A New Antimicrobial Approach to Infectious Disease? *Photochem. Photobiol. Sci.* **2004**, *3*, 436−450.

(11) Li, X.; Lee, D.; Huang, J.-D.; Yoon, J. Phthalocyanine-Assembled Nanodots as Photosensitizers for Highly Efficient Type I Photoreactions in Photodynamic Therapy. *Angew. Chem., Int. Ed.* **2018**, *57*, 9885−9890.

(12) Wang, D.; Niu, L.; Qiao, Z.-Y.; Cheng, D.-B.; Wang, J.; Zhong, Y.; Bai, F.; Wang, H.; Fan, H. Synthesis of Self-Assembled Porphyrin Nanoparticle Photosensitizers. *ACS Nano* **2018**, *12*, 3796−3803.

(13) Li, S.; Cui, S.; Yin, D.; Zhu, Q.; Ma, Y.; Qian, Z.; Gu, Y. Dual Antibacterial Activities of a Chitosan-Modified Upconversion Photodynamic Therapy System Against Drug-Resistant Bacteria in Deep Tissue. *Nanoscale* **2017**, *9*, 3912−3924.

(14) Zhang, Y.; Huang, P.; Wang, D.; Chen, J.; Liu, W.; Hu, P.; Huang, M.; Chen, X.; Chen, Z. Near-Infrared-Triggered Antibacterial and Antifungal Photodynamic Therapy Based on Lanthanide-Doped Upconversion Nanoparticles. *Nanoscale* **2018**, *10*, 15485−15495.

(15) Topaloglu, N.; Gulsoy, M.; Yuksel, S. Antimicrobial Photodynamic Therapy of Resistant Bacterial Strains by Indocyanine Green and 809-nm Diode Laser. *Photomed. Laser Surg.* **2013**, *31*, 155−162.

(16) Topaloglu, N.; Güney, M.; Yuksel, S.; Gülsoy, M. Antibacterial Photodynamic Therapy with 808-nm Laser and Indocyanine Green on Abrasion Wound Models. *J. Biomed. Opt.* **2015**, *20*, 028003.

(17) Luo, S.; Tan, X.; Fang, S.; Wang, Y.; Liu, T.; Wang, X.; Yuan, Y.; Sun, H.; Qi, Q.; Shi, C. Mitochondria-Targeted Small-Molecule Fluorophores for Dual Modal Cancer Phototherapy. *Adv. Funct. Mater.* **2016**, *26*, 2826−2835.

(18) Alves, C. G.; Lima-Sousa, R.; de Melo-Diogo, D.; Louro, R. O.; Correia, I. J. IR780 Based Nanomaterials for Cancer Imaging and Photothermal, Photodynamic and Combinatorial Therapies. *Int. J. Pharm.* **2018**, *542*, 164−175.

(19) Pais-Silva, C.; de Melo-Diogo, D.; Correia, I. J. IR780-Loaded Tpgs-Tos Micelles for Breast Cancer Photodynamic Therapy. *Eur. J. Pharm. Biopharm.* **2017**, *113*, 108−117.

(20) Weng, Y.-H.; Ma, X.-W.; Che, J.; Li, C.; Liu, J.; Chen, S.-Z.; Wang, Y.-Q.; Gan, Y.-L.; Chen, H.; Hu, Z.-B.; Nan, K.-H.; Liang, X.-J. Nanomicelle-Assisted Targeted Ocular Delivery with Enhanced Antiinflammatory Efficacy In Vivo. *Adv. Sci.* **2018**, *5*, 1700455.

(21) Yuan, A.; Qiu, X.; Tang, X.; Liu, W.; Wu, J.; Hu, Y. Self-Assembled PEG-IR-780-C13 Micelle as a Targeting, Safe and Highly-Effective Photothermal Agent for In Vivo Imaging and Cancer Therapy. *Biomaterials* **2015**, *51*, 184−193.

(22) Plenagl, N.; Seitz, B. S.; Reddy Pinnapireddy, S.; Jedelská, J.; Brüßler, J.; Bakowsky, U. Hypericin Loaded Liposomes for Anti-Microbial Photodynamic Therapy of Gram-Positive Bacteria. *Phys. Status Solidi A* **2018**, *215*, 1700837.

(23) Duse, L.; Pinnapireddy, S. R.; Strehlow, B.; Jedelská, J.; Bakowsky, U. Low Level LED Photodynamic Therapy using Curcumin Loaded Tetraether Liposomes. *Eur. J. Pharm. Biopharm.* **2018**, *126*, 233−241.

(24) Ng, V. W. L.; Ke, X.; Lee, A. L. Z.; Hedrick, J. L.; Yang, Y. Y. Synergistic Co-Delivery of Membrane-Disrupting Polymers with Commercial Antibiotics Against Highly Opportunistic Bacteria. *Adv. Mater.* **2013**, *25*, 6730−6736.

(25) Nederberg, F.; Zhang, Y.; Tan, J. P. K.; Xu, K.; Wang, H.; Yang, C.; Gao, S.; Guo, X. D.; Fukushima, K.; Li, L.; Hedrick, J. L.; Yang, Y.-Y. Biodegradable Nanostructures with Selective Lysis of Microbial Membranes. *Nat. Chem.* **2011**, *3*, 409−414.

(26) Liu, Y.; Busscher, H. J.; Zhao, B.; Li, Y.; Zhang, Z.; van der Mei, H. C.; Ren, Y.; Shi, L. Surface-Adaptive, Antimicrobially Loaded, Micellar Nanocarriers with Enhanced Penetration and Killing Efficiency in Staphylococcal Biofilms. *ACS Nano* **2016**, *10*, 4779−4789.

(27) Li, S.; Zhao, Z.; Wu, W.; Ding, C.; Li, J. Dual pH-Responsive Micelles with Both Charge-Conversional Property and Hydrophobic−Hydrophilic Transition for Effective Cellular Uptake and Intracellular Drug Release. *Polym. Chem.* **2016**, *7*, 2202−2208.

(28) Chu, L.; Gao, H.; Cheng, T.; Zhang, Y.; Liu, J.; Huang, F.; Yang, C.; Shi, L.; Liu, J. A Charge-Adaptive Nanosystem for Prolonged and Enhanced In Vivo Antibiotic Delivery. *Chem. Commun.* **2016**, *52*, 6265−6268.

(29) Wu, L.; Wu, M.; Lin, X.; Zhang, X.; Liu, X.; Liu, J. Magnetite Nanocluster and Paclitaxel-Loaded Charge-Switchable Nanohybrids for MR Imaging and Chemotherapy. *J. Mater. Chem. B* **2017**, *5*, 849−857.

(30) Radovic-Moreno, A. F.; Lu, T. K.; Puscasu, V. A.; Yoon, C. J.; Langer, R.; Farokhzad, O. C. Surface Charge-Switching Polymeric

Nanoparticles for Bacterial Cell Wall-Targeted Delivery of Antibiotics. *ACS Nano* **2012**, *6*, 4279−4287.

(31) Feng, T.; Ai, X.; An, G.; Yang, P.; Zhao, Y. Charge-Convertible Carbon Dots for Imaging-Guided Drug Delivery with Enhanced In Vivo Cancer Therapeutic Efficiency. *ACS Nano* **2016**, *10*, 4410−4420.

(32) Yang, H. Y.; Jang, M.-S.; Li, Y.; Fu, Y.; Wu, T. P.; Lee, J. H.; Lee, D. S. Hierarchical Tumor Acidity-Responsive Self-Assembled Magnetic Nanotheranostics for Bimodal Bioimaging and Photo-dynamic Therapy. *J. Controlled Release* **2019**, *301*, 157−165.

(33) Sheppard, J. G.; McAleer, J. P.; Saralkar, P.; Geldenhuys, W. J.; Long, T. E. Allicin-Inspired Pyridyl Disulfides as Antimicrobial Agents for Multidrug-Resistant Staphylococcus Aureus. *Eur. J. Med. Chem.* **2018**, *143*, 1185−1195.

(34) Zhao, X.; Wei, R.; Chen, L.; Jin, D.; Yan, X. Glucosamine Modified Near-Infrared Cyanine as a Sensitive Colorimetric Fluorescent Chemosensor for Aspartic and Glutamic Acid and Its Applications. *New J. Chem.* **2014**, *38*, 4791−4798.

(35) Hu, Q.-J.; Lu, Y.-C.; Yang, C.-X.; Yan, X.-P. Synthesis of Covalently Bonded Boron-Dipyrromethene-Diarylethene for Building a Stable Photosensitizer with Photo-Controlled Reversibility. *Chem. Commun.* **2016**, *52*, 5470−5473.

(36) Pang, X.; Xiao, Q.; Cheng, Y.; Ren, E.; Lian, L.; Zhang, Y.; Gao, H.; Wang, X.; Leung, W.; Chen, X.; Liu, G.; Xu, C. Bacteria-Responsive Nanoliposomes as Smart Sonotheranostics for Multidrug Resistant Bacterial Infections. *ACS Nano* **2019**, *13*, 2427−2438.